JPEDAV (2008) 29:414–428
DOI: 10.1007/s11669-008-9352-6
1547-7037 ©ASM International

On the Quaternary System Ti-Fe-Ni-Al

Xinlin Yan, A. Grytsiv, P. Rogl, V. Pomjakushin, and H. Schmidt

(Submitted November 6, 2007; in revised form April 10, 2008)

The homogeneity ranges of the Laves phases and phase relations concerning the Laves phases in the quaternary system Ti-Fe-Ni-Al at 900 °C were defined by x-ray powder diffraction (XPD) data and electron probe microanalysis (EPMA). Although at higher temperatures the Laves phase forms a continuous solid solution, two separate homogeneity fields of $TiFe_2$-based (denoted by λ_{Fe}) and $Ti(TiNiAl)_2$-based (denoted by λ_{Ni}) Laves phases appear at 900 °C. The relative locations of Laves phases, G phase, Heusler phase, and CsCl-type phase as well as the associated tie-tetrahedra were experimentally established in the quaternary for 900 °C and presented in three-dimensional (3D) view. Furthermore, a partial isothermal section $TiFe_2$-$TiAl_2$-$TiNi_2$ was constructed, and a connectivity scheme, derived for equilibria involving Laves phases in the Ti-Fe-Ni-Al quaternary system at 900 °C was derived. As a characteristic feature of the quaternary phase diagram, the solid solubility of fourth elements in both the $TiFe_2$-based and $Ti(NiAl)_2$-based Laves phases is limited at 900 °C and is dependent on the ternary Laves phase composition. A maximum solubility of about 8 at.% Ni is reached for composition $Ti_{33.3}Fe_{33.3}Al_{33.4}$. Structural details have been evaluated from powder x-ray and neutron diffraction data for (i) the Ti-Fe-Ni ternary and the Ti-Fe-Ni-Al quaternary Laves phases ($MgZn_2$-type, space group: $P6_3/mmc$) and (ii) the quaternary G phase. Atom site occupation behavior for all phases from the quaternary system corresponds to that of the ternary systems. For the quaternary Laves phase, Ti occupies the 4*f* site and additional Ti (for compositions higher than 33.3 at.%Ti) preferably enters the 6*h* site. Aluminum and (Fe,Ni) share the 6*h* and the 2*a* sites. The compositional dependence of unit cell dimensions, atomic coordinates, and interatomic distances for the Laves phases from the quaternary system is discussed. For the quaternary cubic G phase, a centrosymmetric as well as a noncentrosymmetric variety was observed depending on the composition: from combined x-ray and neutron powder diffraction measurements $Ti_{33.33}Fe_{13.33}Ni_{10.67}Al_{42.67}$ was found to adopt the lower symmetry with space group $F\bar{4}3m$.

Keywords crystal chemistry, diffraction (x-ray/neutron powder), intermetallics, phase equilibria, site occupancy, ternary and quaternary titanium aluminides, titanium-iron-nickel-aluminum

1. Introduction

Intermetallic alloys based on the Ti-Fe-Ni-Al system are in the focus of aeroengine applications. Most investigations in the system have been dedicated to improving the alloy properties for desired high-temperature applications. It is well known that properties of alloys are controlled by several factors such as composition, heat treatment, phase constitution, and site occupancies. Therefore, a reliable phase diagram and a complete understanding of phase equilibria in a certain temperature range are important for modern alloy design based on thermodynamic modeling of the constitutional diagram. Recent reviews for the subsystems of the Ti-Fe-Ni-Al quaternary provide such information.[1-15] However, on the extension from the ternary systems to the quaternary system, there are only few investigations available in literature.[16-24] Past efforts associated with the quaternary system include: (i) the relation between structure and magnetic properties of a magnetically semipermanent alloy with specific compositions Fe-(10-25)Ni-(3-5)Al-1Ti (wt.%),[16] Fe-18Ni-3.8 Al-1Ti (wt.%),[17] Fe-13.8Ni-7.0Al-1.7Ti (at.%),[18] and Fe-16.2Ni-3.1Al-1.13Ti (wt.%),[19] (ii) alloying effects on superplastic behavior for Ti-based alloys Ti-5Fe-*x*Al-*y*Ni (x = 4-8, y = 0, 1, or 2) (wt.%),[22] (iii) phase relation between CsCl-type and Heusler phases within the NiAl-TiNi-TiFe-FeAl section,[21] (iv) Partitioning behavior of alloying elements among the phases of γ', η, β_1, β_2, and H in the Ni-Al-Ti base systems,[23] and (v) the effect of Ti additions on the microstructure of Ni-Al-Fe alloys.[20]

In this work, we evaluate the homogeneity regions of the quaternary Laves phase with $MgZn_2$-type structure in continuation of our investigation on the ternary Laves phases Ti-Fe-Al[25] and Ti-Ni-Al.[26] Several researchers[4,9,27-29] have dealt with the phase diagram Ti-Fe-Al, in which a large solid solubility of Al in the binary Laves phase $TiFe_2$ exists. Almost 33.5 at.% Fe can be replaced by Al at 800 °C, and a value of 47 at.% can be reached at 1000 °C.[28] In a previous work, we showed that Al

Xinlin Yan, A. Grytsiv, P. Rogl, and **H. Schmidt**, Institute of Physical Chemistry, University of Vienna, Währingerstrasse 42, A-1090 Wien, Austria; and **V. Pomjakushin,** Laboratory for Neutron Scattering, ETH Zurich & Paul Scherrer Institut, CH-5232 Villigen PSI, Switzerland. Contact e-mails: peter.franz.rogl@univie.ac.at, andriy.grytsiv@univie.ac.at, and yanxinlin13@hotmail.com.

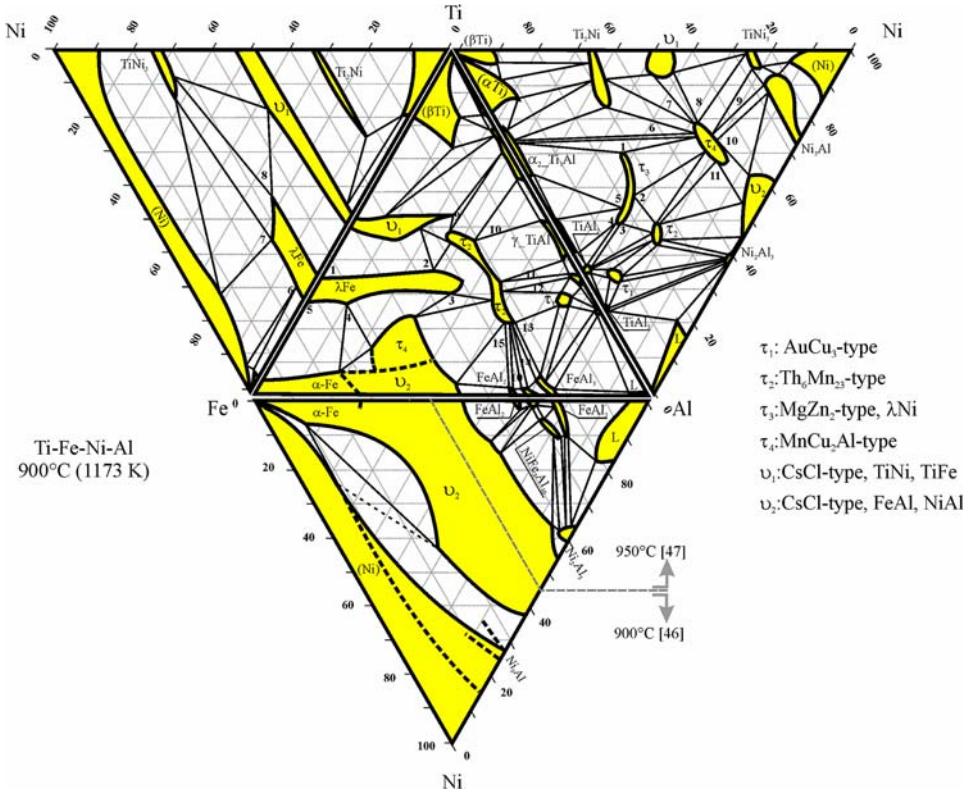

Fig. 1 Literature data on ternary subsystems of Ti-Fe-Ni-Al quaternary system

substitution takes place on two crystallographically different Fe positions simultaneously.[26] Determination of phase relations in the system Ti-Ni-Al[30-32] revealed a large homogeneity region for the ternary Laves phase with $MgZn_2$-type structure: $Ti(Ti_yNi_xAl_{1-x-y})_2$. The "boomerang-like" shape of the phase field in the isothermal section at 900 °C was defined by Grytsiv et al.,[26] indicating a complicated atom site exchange mechanism. In the Ti-Fe-Ni system;[14,33] the solid solubility of Ni in $TiFe_2$ was found to be very large too, at around 23 at.% at 900 °C. However, to our knowledge, there is no report about the existence of a Ni-Fe-Al Laves phase in literature.

Structural details of the Heusler phase ($MnCu_2Al$-type) and G phase (Th_6Mn_{23}-type) in the quaternary system are equally important with respect to physical properties[21,34,35] as the atom's environment in the unit cell directly influences macrophysical properties of materials.[36] It is interesting to note that for the G phase in the ternary Ti-Fe-Al system, two-phase fields exist corresponding to the Ti-rich side and Al-rich side, respectively.[9,28] Our previous work defined the structure varieties,[35,37,38] that is, the loss of symmetry in the G phase as a function of composition resulting in a space group change from $Fm\bar{3}m$ (Al-rich) to $F\bar{4}3m$ (Al-poor).[35] In a previous investigation on a series of alloys $Ti(Fe_{50-x}Ni_x)Al$, we elucidated atom site preferences for the Heusler phase in the quaternary system.[39]

The purpose of the present work is (i) to clarify the homogeneity region of Laves phases in the quaternary system Ti-Fe-Ni-Al at 900 °C, (ii) to define phase equilibria in which the Laves phase is involved at 900 °C, and (iii) to determine the site occupancy of atoms in the quaternary phases, namely the Laves phase $Ti(Ti,Fe,Ni,Al)_2$ with $MgZn_2$-type and the G phase with a Th_6Mn_{23}-derivative type structure.

2. Experiment Details

More than 120 alloys with a weight of 1 g were prepared by argon arc melting from high-purity materials (more than 99.9 mass%) on a water-cooled copper hearth (quenching rate >100 °C/s). The locations of the investigated alloys were selected to establish the homogeneity range of the Laves phases in the quaternary system. To ensure homogenization, all alloys were remelted three times. A part of each alloy was vacuum sealed in quartz tubes and annealed at 900 °C for 10 days before being quenched in cold water. X-ray powder diffraction (XPD) data from as-cast and annealed samples were collected employing a Guinier-Huber image plate system with Cu $K\alpha_1$ or Fe $K\alpha_1$ ($8° < 2\theta < 100°$). Precise lattice parameters were calculated by least-squares fits to indexed 4θ values employing Ge as internal standard ($a_{Ge} = 0.5657906$ nm). X-ray powder intensity data for the determination of structural parameters were collected on a Siemens D5000 instrument with Cu $K\alpha_{1,2}$ ($10° < 2\theta < 110°$, step $(2\theta) = 0.02°$) equipped with an energy dispersive SOLX detector.

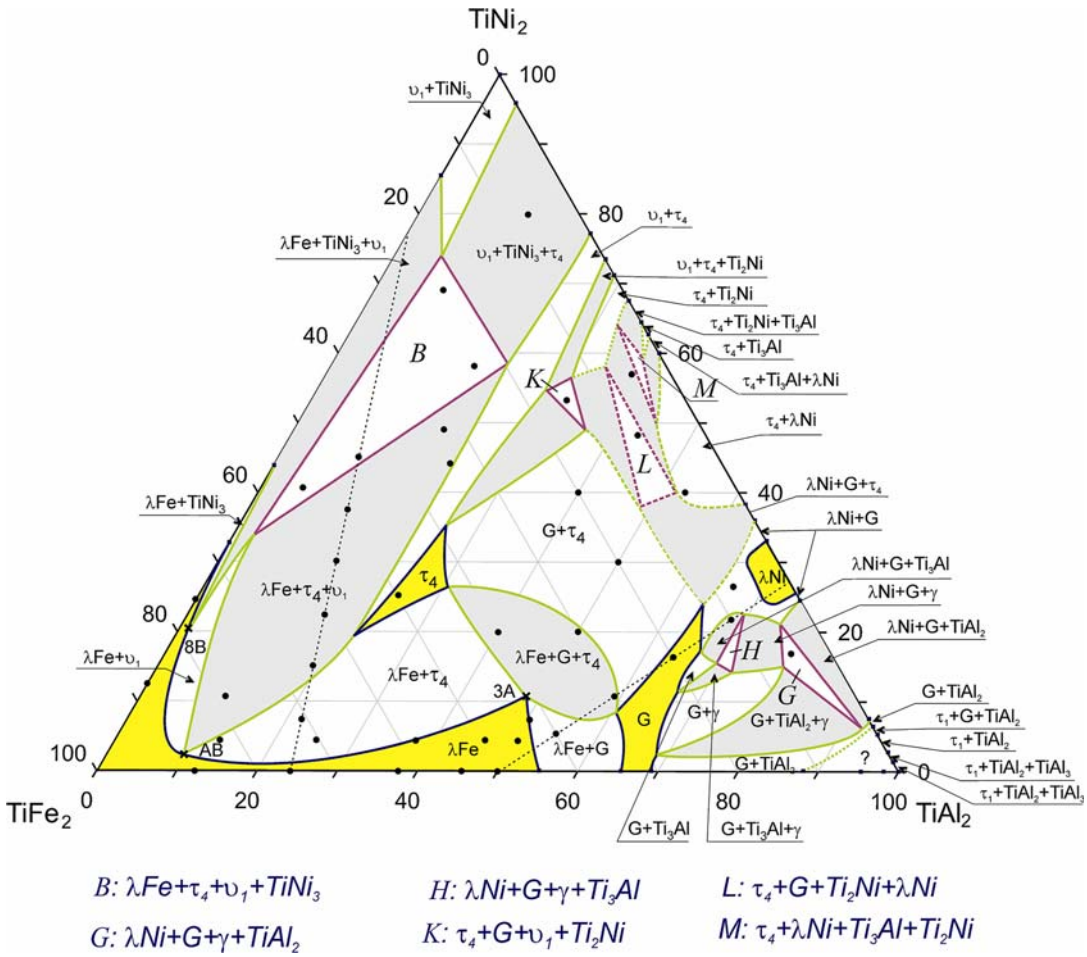

Fig. 2 Partial $TiFe_2$-$TiAl_2$-$TiNi_2$ isothermal section at 900 °C

Neutron diffraction experiments were performed in high-intensity mode ($\Delta d/d \geq 2\times10^{-3}$) on the high-resolution powder diffractometer (HRPT)[40] at the SINQ spallation source of the Paul Scherrer Institute, Switzerland. To reduce preferential orientation effects, the alloys were powdered to a grain size below 60 μm. The neutron wavelength used in the present measurements is $\lambda_{neutron}$ = 0.18857 nm and the θ range was 5° ≤ 2θ ≤ 165°.

Single crystals were mechanically isolated from the crushed alloy. Inspection on an AXS-GADDS texture goniometer ensured high crystal quality, unit cell dimensions, and Laue symmetry of the specimens prior to x-ray intensity data collection on a four-circle Nonius Kappa diffractometer equipped with a CCD area detector and employing graphite monochromated Mo Kα radiation (λ = 0.071073 nm). Orientation matrix and unit cell parameters for a cubic system were derived using the program DENZO.[41] No absorption corrections were necessary because of the rather regular crystal shape and small dimensions of the investigated specimens. The structures were solved by direct methods and refined with the SHELXL-97 and SHELXS-97 program.[42]

Quantitative Rietveld refinement of the x-ray and neutron powder diffraction data was performed with the FULLPROF program,[43] employing internal tables for neutron scattering lengths and x-ray atomic form factors.

All as-cast and annealed samples were polished via standard procedures and have been examined by optical metallography and scanning electron microscopy (SEM). Specimen compositions were determined by electron probe microanalysis (EPMA) on a Carl Zeiss DSM 962 instrument equipped with a Link EDX system operated at 20 kV and 60 μA.

3. Ternary Subsystems

Literature data on the ternary boundary systems were selected to serve as a basis for the homogeneity regions of the Laves phases in the quaternary system at 900 °C and for the construction of the isothermal section $TiFe_2$-$TiAl_2$-$TiNi_2$.

The isothermal section at 900 °C of the Ti-Fe-Al system was accepted from Palm et al.[28] in a recently assessed and updated version by Palm and Lacaze.[9] Various assessments are available for the Ti-Ni-Al system[3,12,13] and backed by new experimental data on alloys annealed at 900 °C in well-calibrated thermal environment; our previous results on the

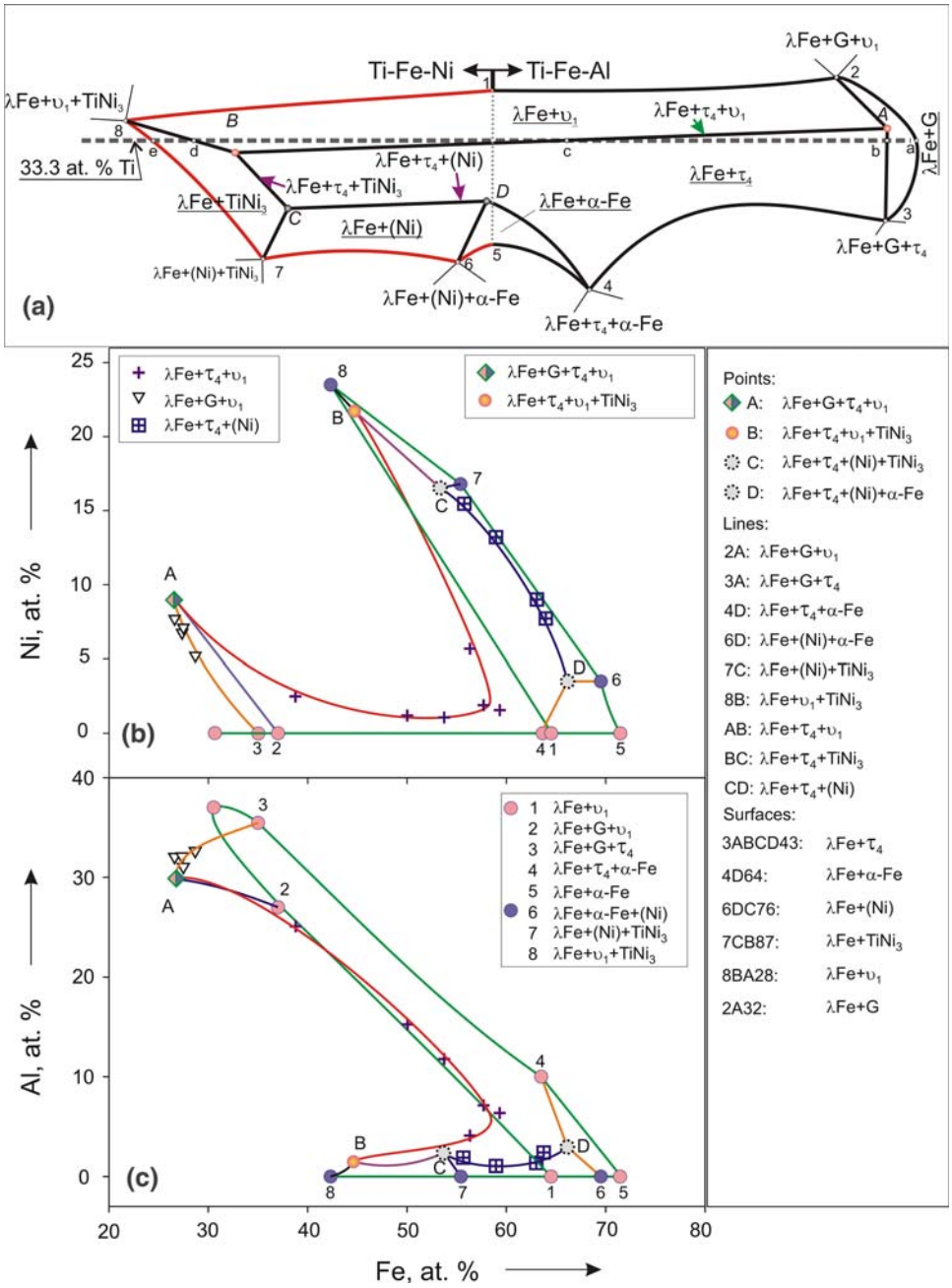

Fig. 3 Schematic phase equilibria (a) associated with λ_{Fe} and projections of homogeneity region in Ni-Fe (b) and Al-Fe (c) directions. Dotted circles denote estimated compositions

isothermal section at 900 °C[32] and on the Ti-Ni-Al Laves phase[26] are retained for the present work. The Ti-Fe-Ni isothermal section at 900 °C from van Loo et al.[44] was used. For more details about this system, the reader is referred to Ref 2, 11, 14, 33, and 45. For the system Fe-Ni-Al there is no complete isothermal section at 900 °C in the literature; therefore, the partial isothermal section for the Al-poor side at 900 °C[46] was combined with a partial isothermal section covering the Al-rich side at 950 °C.[47] The latest assessment can be found in Ref 8 and 10. Figure 1 presents all four subsystems of the Ti-Fe-Ni-Al quaternary system.

4. Results and Discussion

According to Gibbs's phase rule, a four-component system may engage in isothermal reactions with five phases at a characteristic pressure and temperature. The

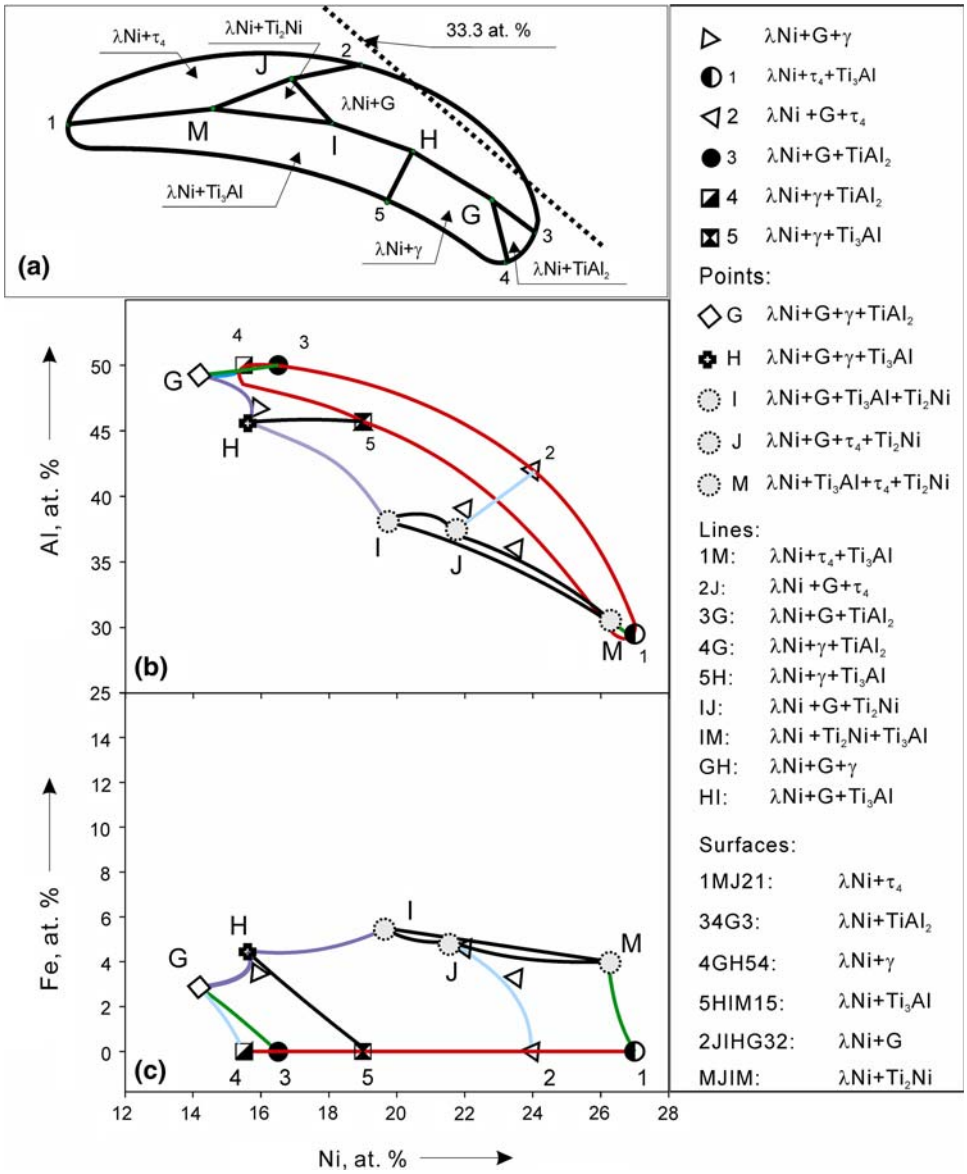

Fig. 4 Schematic phase equilibria (a) associated with λ_{Ni} and projections of homogeneity region in Ni-Al (b) and Fe-Ni (c) directions. Dotted circles denote estimated compositions

convenient way to present a quaternary system at constant *P*,*T* is the composition tetrahedron (Roozeboom-Fedorov tetrahedron; simplex). Depending on the type of isothermal-isobaric reaction, the sequence of four-phase tie-tetrahedra through the reaction differs. For correct construction of phase relations among the tie-tetrahedra and the adjoining phase fields, the rule of Palatnik and Landau[48] on the association of phase fields may be applied. On many occasions, the rule helps to define missing phase fields and their proper phase constituents and to link tie-tetrahedra from different reactions via proper three- and two-phase regions. Generally, a multicomponent phase diagram of any order may be presented by definition of two types of phase regions: single-phase regions and invariant tie-tetrahedra. All other phase fields with intermediate numbers of equilibrium phases may be derived from the phase rule. The invariant tie-tetrahedron has a simple shape defined by the compositions of the equilibrium phases, while phase fields of lower index have a complicated shape that is mainly defined by the respective single-phase regions.

4.1 Homogeneity Regions for the Quaternary Laves Phases

In order to determine the single-phase regions for Laves phases in the Ti-Fe-Ni-Al system at 900 °C, first investigations were performed for alloys at a constant content of 33.3 at.% Ti (Fig. 2 presents phase regions that are discussed in detail in section 4.2.1.). Electron probe

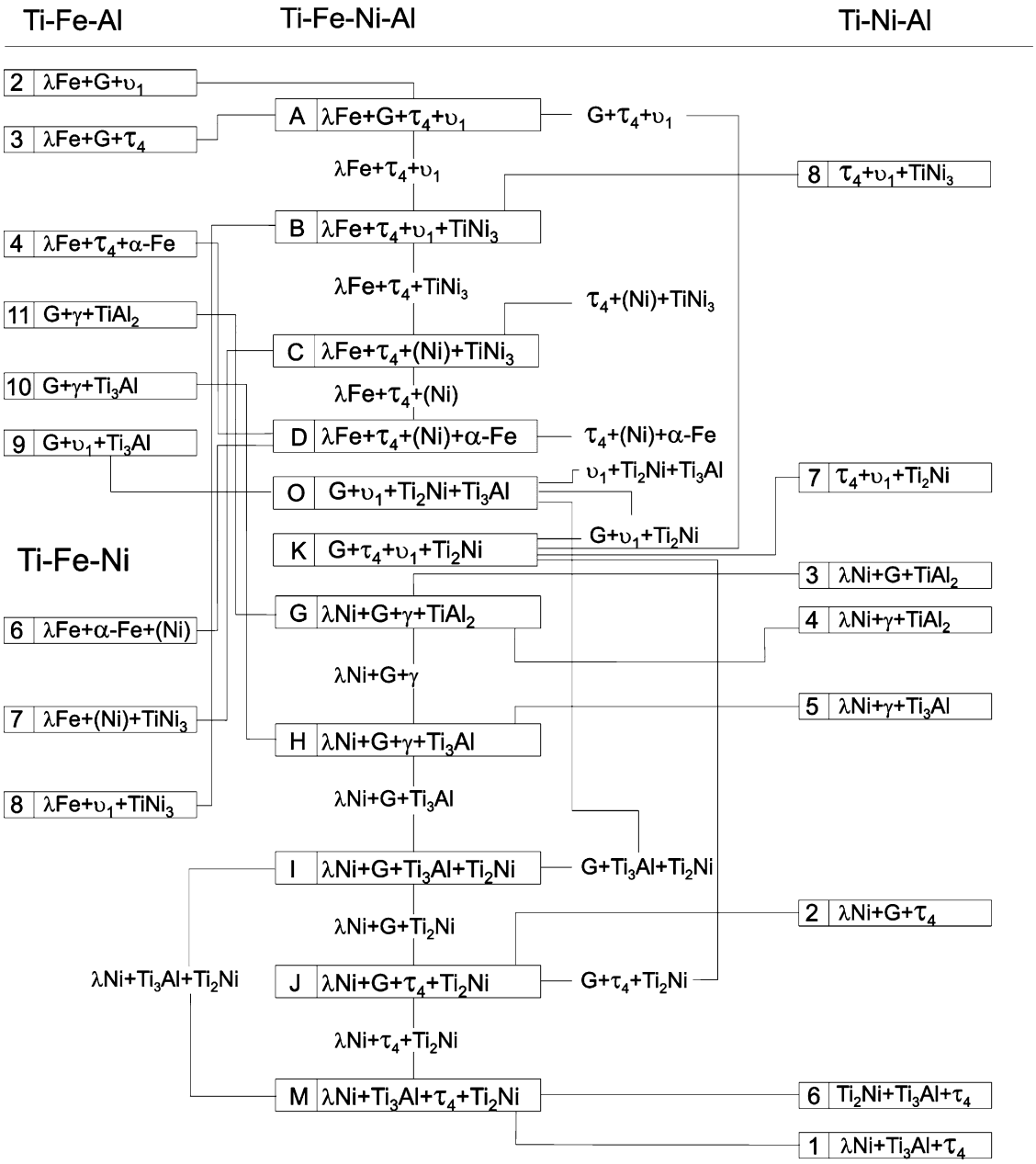

Fig. 5 Connectivity scheme in the Ti-Fe-Ni-Al quaternary system at 900 °C for equilibria involving Laves phases

microanalysis (EPMA) and XPD data for alloys in the as-cast state and after anneal at 900 °C evidence that Laves phases exhibit extensive single-phase fields in alloys quenched from melt (as-cast), but homogeneity regions appear significantly reduced at 900 °C. For example, alloys from the series $Ti(Fe_{0.5}Al_{0.5})_2$-$Ti(Fe_{0.45}Ni_{0.45}Al_{0.1})_2$ are single-phase Laves phase in the as-cast condition while anneal at 900 °C reveals the formation of a G phase (τ_2). The small solubility of the fourth component (less than 4 at.%) in the $TiFe_2$-based Laves phase is also observed from investigations of $Ti(Fe_{0.75}Al_{0.25})_2$-$Ti(Fe_{0.45}Ni_{0.45}Al_{0.1})_2$ alloys where the Laves phase was found in equilibrium with Heusler phase or/and CsCl-type structure (υ_1).

λ_{Fe} and λ_{Ni} do not form a continuous solid solution at 900 °C due to the competitive formation of a continuous solid solution of the G phase (τ_2) connecting the ternary systems Ti-Fe-Al and Ti-Ni-Al. Furthermore, the extent of the homogeneity region of λ_{Fe} is strongly reduced by the emerging Heusler phase in the Ti 33.3 at.% section. Compositions of Laves phases (λ_{Fe} and λ_{Ni}) at 900 °C are plotted in Fig. 3 and 4 to outline the single-phase regions of these phases and to estimate the compositions of phases involved in four-phase equilibria. Figure 3 and 4 show vertices (points), lines, and surface areas associated with the Laves phases in two-dimensional (2D) projections (in certain directions) of the three-dimensional quaternary phase

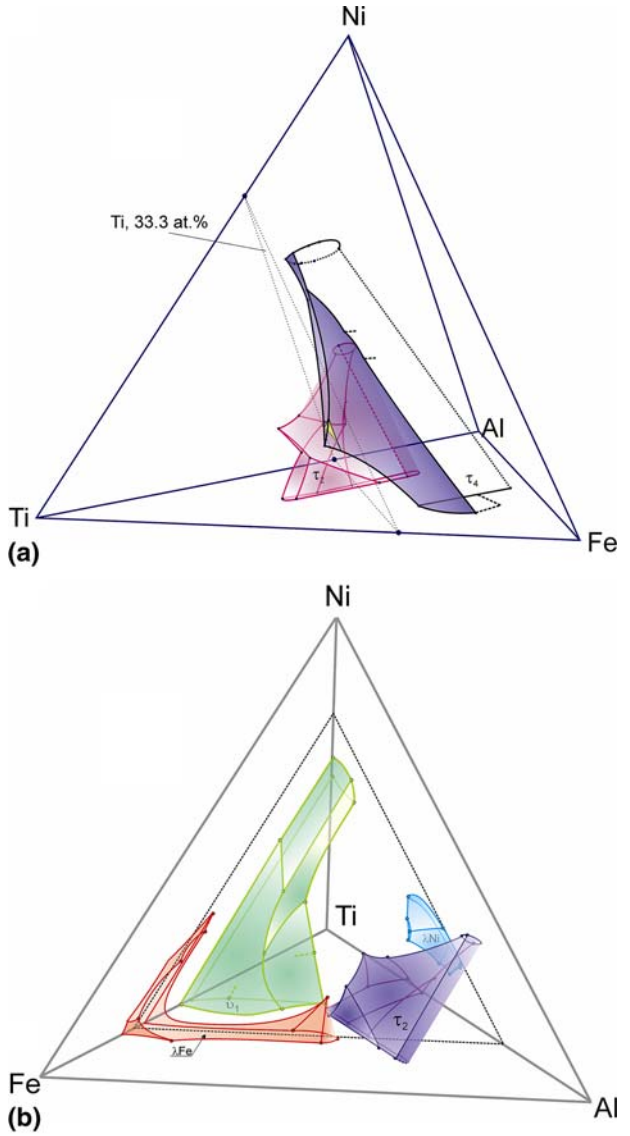

Fig. 6 3D view of homogeneity regions in the Ti-Fe-Ni-Al phase diagram at 900 °C: (a) of τ_2 and τ_4, the 33.3 at.% Ti section is outlined with dots to reveal the deviation of the Heusler phase from Ti 25 at.%, (b) of the Laves phases, τ_2 and υ_1 phases

diagram. The right part of the figure contains the legend to these points, lines, and areas formed by the respective phases. Laves phase compositions from two-phase alloys are not presented in these figures to avoid confusion with those from three- or four-phase equilibrium alloys. The compositions from three- or four-phase equilibrium alloys basically shape the homogeneity ranges of the Laves phases with additional data derived from the ternary phase diagrams (denoted using the corresponding numbers as used in Fig. 1). Projections of the Laves phase regions and the connectivity scheme in Fig. 5 served in all steps of experiments as a tool to check four-phase equilibria and thereby warrant that no vertices for single-phase regions on the Laves phase surface are missing. Due to the complexity of visualization of the four-component phase diagram, additional tests were performed (i) to ensure the consistency of EPMA, (ii) to avoid intersection among four-phase tie-tetrahedra, and (iii) to exclude penetration of invariant tie-tetrahedra and single-phase regions. For this purpose, a computer program was written and program Atoms[49] was used for visualization of tie-tetrahedra in 3D space. Based on these examinations, subsequent series of alloys were defined to establish the extensions of the Laves phase regions and to localize all four-phase equilibria involving these phases. As a final result, a three-dimensional (3D) view of single-phase regions for both Laves phases is presented in Fig. 6, and data on phases coexisting in invariant equilibria at 900 °C are listed in Table 1. The solid solubility of the fourth element in both ternary Laves phases is limited at 900 °C and is strongly composition dependent. The maximum Ni solubility in λ_{Fe} is reached at about 8 at.% (point A), but only about 5 at.% Fe can be dissolved in λ_{Ni} (point I) (see Table 1, Fig. 3 and 4). Finally, it should be noted that phase boundary lines are defined to an accuracy of better than ±3 at.%.

4.2 Phase Equilibria in the Quaternary System

4.2.1 The section $TiFe_2$-$TiAl_2$-$TiNi_2$ at 900 °C. The section $TiFe_2$-$TiAl_2$-$TiNi_2$, shown in Fig. 2 and accompanied by a connectivity scheme in Fig. 5, elucidates equilibria involving the Laves phases in the quaternary system. One can see that phase equilibria with the Heusler phase (τ_4), the G phase (τ_2), and the CsCl-type phase (υ_1) dominate the section. As a consequence, it is interesting to note that isostructural λ_{Fe} and λ_{Ni} do not form a continuous solid solution at 900 °C. Phase relations in the region of λ_{Fe} are rather simple, whereas complex phase relations are observed for λ_{Ni}, particularly in the $TiAl_2$ corner of the section. The existence of the Heusler phase at 33.3 at.% Ti is surprising, taking into account that the titanium content in this structure typically does not exceed 25 at.%. Details on the crystal structure of this phase for compositions $Ti_{33.3}Fe_{33.3}Ni_{16.7}Al_{16.7}$ (Ti_2Fe_2NiAl) and $Ti(Fe,Ni)_2Al$ have been discussed.[39] Despite the limited amount of experimental data, the positions of the tie-tetrahedra B, G, and H in the $TiFe_2$-$TiAl_2$-$TiNi_2$ section are well established, allowing only little speculation for their connection with respective phase fields in the boundary systems Ti-Fe-Ni and Ti-Ni-Al. The section $TiFe_2$-$TiAl_2$-$TiNi_2$ does not represent all equilibria established for the Ti-Fe-Ni-Al quaternary as some of the invariant tie-tetrahedra are not cut by this section. Numerical information on composition of equilibrium phases (Table 1) and the connectivity scheme (Fig. 5) serve as a good starting point for visualization of the phase equilibria in terms of a 3D view of the Ti-Fe-Ni-Al phase diagram at 900 °C.

4.2.2 Three-Dimensional Presentation of the Ti-Fe-Ni-Al Phase Diagram for 900 °C. Figure 6 to 7, 8 show in 3D fashion the phase relations at 900 °C in the quaternary system among λ_{Fe} and λ_{Ni}, τ_2, τ_4 and υ_1. The connectivity scheme plays a crucial key as a guideline to complete the construction of the 3D quaternary phase diagram. Single-phase regions and tie-tetrahedra were controlled with respect to their relative positions in space using the 3D program "Atoms" to fulfill the fundamental phase rule; for

Table 1 Phase analysis for annealed samples (900 °C) with four-phase equilibria in the quaternary system Ti-Fe-Ni-Al by EPMA and XPD

	EMPA(a), at.%						Lattice parameters, nm	
Tie-tetrahedra	Ti	Fe	Ni	Al	Phase analysis	Structure type	*a*	*c*
A	41.0	21.2	8.7	29.1	G	$Mn_{23}Th_6$	1.20284(5)	···
	37.9	31.1	13.1	17.9	τ_4	$MnCu_2Al$	0.59210(5)	···
	45	32	13	10	υ_1	CsCl	0.29831(4)	
	34	28	8	30	λFe	$MgZn_2$	0.49489(8)	0.79815(9)
B	28.0	9.5	44.4	18.1	τ_4	$MnCu_2Al$	0.59103(9)	
	23.5	6.5	67.3	2.7	$TiNi_3$	Cu_3Au	0.51220(4)	0.83443(5)
	46	22	26	6	υ_1	CsCl	0.29741(5)	
	33.2	44.6	21.7	0.5	λFe	$MgZn_2$	0.47870(6)	0.77925(9)
C	24.1	18.9	35.7	21.3	τ_4	$MnCu_2Al$	0.5799(4)	···
	8	60	25	7	(Ni)	Cu	0.36083(6)	···
	23	8	67	2	$TiNi_3$	Cu_3Au	0.51757(1)	0.83780(3)
	27	54	16	3	λFe	$MgZn_2$	0.47676(9)	0.77709(9)
D	23	25	31	21	τ_4	$MnCu_2Al$	0.5757(6)	···
	7	75	15	3	(Ni)	Cu	0.3497(2)	···
	4	93	2	1	α-Fe	W		···
	26	67	4	3	λFe	$MgZn_2$	0.47803(3)	0.7787(4)
O	55	9	20	16	Ti_2Ni	Ti_2Ni	1.1255(1)	···
	73	1	1	25	Ti_3Al	Mg_3Cd	0.57818(4)	0.4644(1)
	50	21	12	17	υ_1	CsCl	···	···
	42	17	8	33	G	$Mn_{23}Th_6$	1.20797(4)	···
K	44.2	13.5	14.2	28.1	G	$Mn_{23}Th_6$	0.59099(4)	···
	28.1	7.8	41.6	22.5	τ_4	$MnCu_2Al$	1.20652(4)	···
	45.5	19.1	24.2	11.2	υ_1	CsCl	0.30214(1)	···
	51.7	10.2	22.7	15.4	Ti_2Ni	Ti_2Ni	1.12247(9)	···
G	27.5	8	15.4	49.1	G	$Mn_{23}Th_6$	1.19688(9)	···
	41.4	0.2	2.1	56.3	γ	CuAu	Trace	
	34.0	0.3	2.7	63.0	$TiAl_2$	$ZrGa_2$	Trace	
	33.7	2.9	14.2	49.2	λNi	$MgZn_2$	0.50271(2)	0.82342(6)
H	29	11.5	11.5	48	G	$Mn_{23}Th_6$	1.20213(1)	···
	50.0	1.3	2.2	46.5	γ	CuAu	0.39679(1)	0.40886(1)
	63	1	1	35	Ti_3Al	Mg_3Cd	Trace	
	34.2	4.4	15.6	45.8	λNi	$MgZn_2$	0.4785(4)	0.7756(9)
I	34	11	13	42	G	$Mn_{23}Th_6$	1.20560(5)	···
	67	1	1	31	Ti_3Al	Mg_3Cd	0.57810(4)	0.46403(5)
	50	9	20	21	Ti_2Ni	Ti_2Ni	···	···
	37	6	20	37	λNi	$MgZn_2$	0.50115(5)	0.80795(9)
J	39	11	15	35	G	$Mn_{23}Th_6$	1.20502(4)	···
	24	5	43	28	τ_4	$MnCu_2Al$	0.58954(4)	···
	60	6	26	8	Ti_2Ni	Ti_2Ni	1.12244(6)	···
	36	5	22	37	λNi	$MgZn_2$	0.49999(4)	0.80513(8)
M	27	2	46	25	τ_4	$MnCu_2Al$	···	···
	58	4	28	10	Ti_2Ni	Ti_2Ni	1.12180(7)	···
	70	1	1	28	Ti_3Al	Mg_3Cd	0.57926(6)	0.46557(9)
	38	4	24	34	λNi	$MgZn_2$	0.50151(4)	0.80816(5)

(a) Integer values for composition correspond to estimated or measured by EPMA with low reliability

example, any two tie-tetrahedra cannot intersect each other. The general rules for phase field connection in a four-component system imply that two-, three-, and four-phase regions are connected to a single-phase body via corresponding surfaces, lines, and vertices, respectively, as illustrated for the Laves phases in Fig. 3 and 4. Points of four-phase equilibria (e.g., "A", which in Fig. 3 appears as the vertex where the tie-tetrahedron A representing the four-phase equilibrium A connects with the Laves phase surface; see also Fig. 6 to 8) are connected with the respective three phase fields (e.g., "2" and "3" in the Ti-Fe-Al system and "λFe + τ_4 + υ_1"; see Fig. 1 and 4).

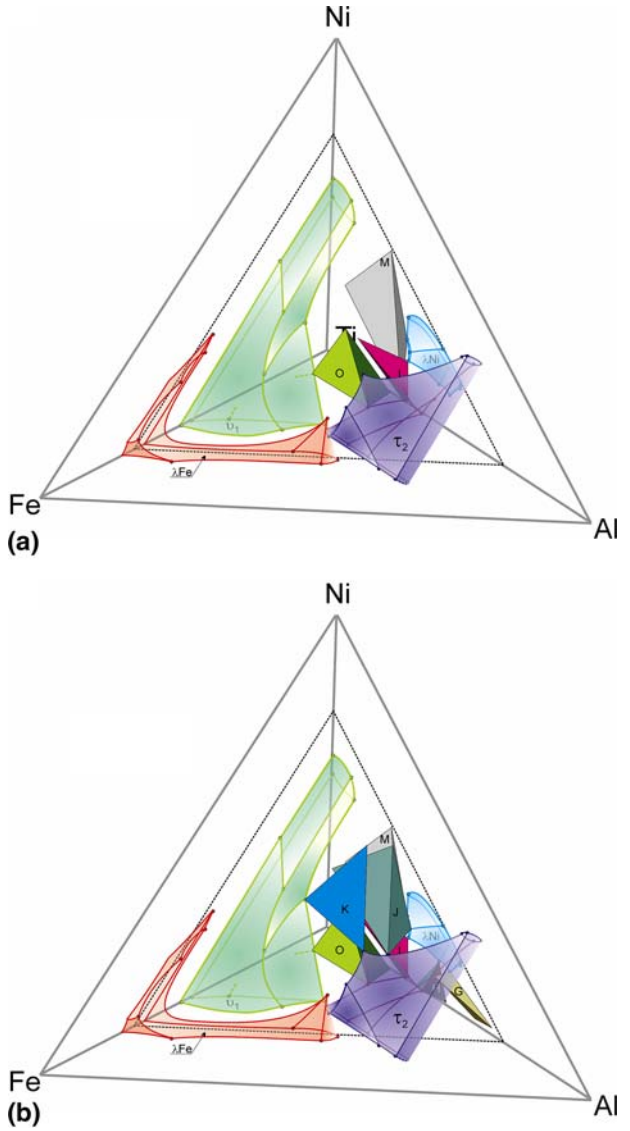

Fig. 7 3D view of homogeneity regions and tie-tetrahedra in the Ti-Fe-Ni-Al phase diagram at 900 °C without (a) or with (b) the incorporation of certain tie-tetrahedra

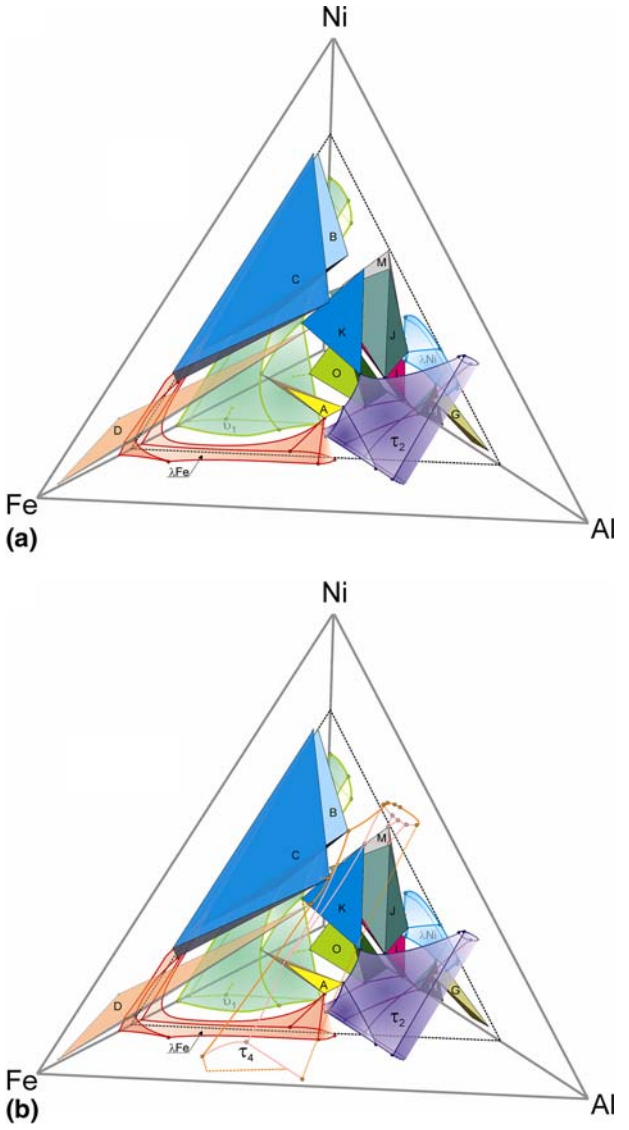

Fig. 8 3D view of homogeneity regions and tie-tetrahedra in the Ti-Fe-Ni-Al phase diagram at 900 °C without (a) or with (b) the presentation of the τ_4 single-phase volume

Although in Fig. 6 to 8 only single-phase regions and tie-tetrahedra are presented, three phase equilibrium areas essentially can be defined by connecting the corresponding faces of invariant tetrahedra by volumes that are formed by ruled surfaces. The ruled surfaces are defined by respective lines on the single-phase regions. For both Laves phases the 3D position of these lines can be read from Fig. 3 and 4. The remaining volumes after visualization of single-, four-, and three-phase equilibria are two-phase equilibrium volumes.

Figure 6(b) to 8 are made from the same viewpoint but switch on or off certain phases and tie-tetrahedra to visualize the shapes, positions, and the relations among single-phase regions and tie-tetrahedra. From Fig. 6 to 8 one can easily extract the main characteristic of the quaternary system, that is, that the two kinds of Laves phases are isolated by the τ_2 phase. In the Ti-Fe-Al ternary the G phase region is split by the Laves phase at high temperature (isothermal section at 1000 °C) into two separate phase fields.[9,28] Such a behavior would also be expected in the quaternary system and indeed is found from the alloy series $Ti(Fe_{0.5-0.1x}Ni_{0.055x}Al_{0.5+0.045x})_2$ ($0 \le x \le 5$). X-ray powder diffraction and EPMA disclosed that these alloys are single-phase Laves type in the as-cast condition, but single-phase G-type or multiphase at 900 °C (Laves phase in equilibrium with G phase). This information suggests that the two Laves phases would join at a certain temperature above 900 °C to form a continuous solid solution splitting the G phase region (that forms a continuous solid solution at 900 °C).

To illustrate the shape of the Heusler phase single-phase volume, another visual angle as shown in Fig. 6(a) is selected to present the 3-D phase diagram (only Heusler phase, G phase single-phase volumes and Ti 33.3 at.%

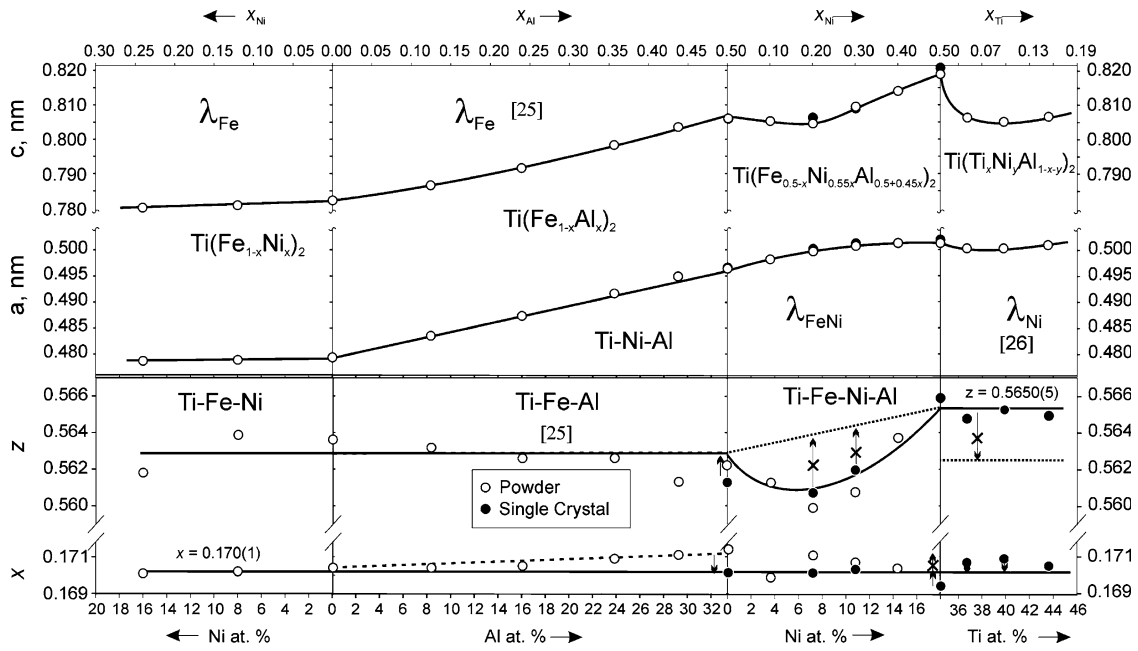

Fig. 9 Compositional dependencies of lattice and atomic position parameters for binary-, ternary- and quaternary- Laves phases versus concentration

section are presented). The Heusler phase with the anomalous shape strongly suppresses the solid solubility of Ni in λ_{Fe}, which is directly reflected by the shape of the λ_{Fe} single-phase volume [see Fig. 6(b)].

4.3 Crystal Chemistry

4.3.1 $MgZn_2$-Type Laves Phases. The continuous solid solution of the Ti-Fe-Ni-Al Laves phase (denoted as λ_{FeNi}) observed in as-cast alloys has split into two independent nonconnected single-phase regions at 900 °C (λ_{Fe} and λ_{Ni}). To elucidate details on atom site preference and bonding characteristics of the Laves phase in the quaternary system, three sets of alloys representing λ_{FeNi}, λ_{Fe}, and λ_{Ni} were used for structural investigations. Due to the limited solubility of a fourth component in λ_{Fe} at 900 °C, structural details of this solid solution are discussed on the basis of ternary data for $Ti(Fe_{1-x}Al_x)_2$[25] and new data for $Ti(Fe_{1-x}Ni_x)_2$ obtained in the current investigation. The crystal chemistry of λ_{Ni} was outlined by Grytsiv et al.[26] The true quaternary Laves phases λ_{FeNi} are presented by as-cast alloys prepared between λ_{Fe} and λ_{Ni} with compositions $[Ti(Ni_{0.27}Al_{0.73})_2]$ and $[Ti(Fe_{0.5}Al_{0.5})_2]$. Figure 9 summarizes the structural details for ternary and quaternary alloys.

The $TiFe_2$-Based Laves Phase (λ_{Fe}). To complement our structural investigation for the Ti-Fe-Ni-Al $MgZn_2$-type Laves phase, two alloys from the Ti-Fe-Ni subsystem with compositions $Ti_{33.3}Fe_{58.7}Ni_8$ and $Ti_{33.3}Fe_{50.7}Ni_{16}$ were studied. Both alloys were annealed at 900 °C, and EPMA measurements reveal an almost single-phase Laves phase with only a tiny amount of secondary Ti_2Ni (Ti_2Ni-type). Table 2 summarizes the x-ray Rietveld refinement results. Similar to the $MgZn_2$-type Laves phase in the subsystems Ti-Fe-Al[25] and Ti-Ni-Al,[26] the Ti-Fe-Ni Laves phase adopts Ti in the 4*f* site. X-ray diffraction is not sensitive enough to distinguish between Fe and Ni atoms located in the 2*a* and 6*h* sites. However, the shape of the single-phase region in the Ti-Fe-Ni system at 900 °C[44] implies substitution of Fe by Ni. Consistent with the difference of the atomic radii of Ni and Fe [r_{Ni} = 1.246 nm; r_{Fe} = 1.274 nm (CN = 12)], this replacement results in lattice parameters shrinking with Ni content (Fig. 9, Table 2). The smaller lattice parameters and positional parameter *z* of $Ti_{33.3}Fe_{50.7}Ni_{16}$ compared with $Ti_{33.3}Fe_{58.7}Ni_8$ are essentially reflected by the interatomic distances of $d_{Ti\text{-}3Ti}$ and $d_{Ti\text{-}1Ti}$ (see Table 2). It is interesting to note that $d_{Ti\text{-}1Ti}$ for the Ni-rich composition $Ti_{33.3}Fe_{50.7}Ni_{16}$ appears to be higher than $d_{Ti\text{-}3Ti}$, while a reverse situation is observed for all other investigated alloys.

Although substitution of Fe atoms by much bigger Al atoms (r_{Al} = 0.1432 nm) is reflected by a higher slope of the lattice parameters versus Al-content, positional parameters for λ_{Fe} do not change significantly (Fig. 9).

The Quaternary Laves Phase (λ_{FeNi}). Three alloys $Ti_{33.7}Fe_{13.3}Ni_{10.8}Al_{42.2}$, $Ti_{34.9}Fe_{13.3}Ni_{14.4}Al_{37.4}$, and $Ti_{37.4}Fe_{13.3}Ni_{16.2}Al_{33.1}$ from the quaternary system were selected for structural investigation. X-ray powder diffraction data and EPMA measurements on the as-cast alloys reveal that $Ti_{33.7}Fe_{13.3}Ni_{10.8}Al_{42.2}$ is single-phase Laves-type, while the others show a small amount of secondary phases (Table 3). Structure models proved to be suitable with reasonable residual values and moderate thermal displacement values in each position as shown in Table 3. Rietveld refinements employing various models for atom site occupation as

Table 2 Structural data for ternary Ti-Fe-Ni Laves phase ($MgZn_2$-type, space group: $P6_3/mmc$) alloys (Data collection: D5000; Radiation: Cu Kα; 2θ range: 18 ≤ 2θ ≤ 110) (a)

Parameter/Compound	$Ti_{33.3}Fe_{58.7}Ni_8$	$Ti_{33.3}Fe_{50.7}Ni_{16}$
Heat treatment	900 °C	900 °C
a, nm, Guinier	0.47888(2)	0.47875(2)
c, nm, Guinier	0.78077(4)	0.78013(8)
V, nm^3	0.15506(1)	0.15485(2)
ρ_x, Mg/m^3	6.87	6.90
Reflections used in refinement	53	55
Number of variables	25	23
$R_F = \Sigma\lvert F_o - F_c\rvert/\Sigma F_o$	0.088	0.081
$R_I = \Sigma\lvert I_o - I_c\rvert/\Sigma I_o$	0.075	0.071
$R_{wP} = [\Sigma w_i\lvert y_{oi} - y_{ci}\rvert^2/\Sigma w_i\lvert y_{oi}\rvert^2]^{1/2}$	0.124	0.070
$R_P = \Sigma\lvert y_{oi} - y_{ci}\rvert/\Sigma\lvert y_{oi}\rvert$	0.097	0.053
$R_e = [(N - P + C)/(\Sigma w_i y^2_{oi})]^{1/2}$	0.055	0.036
$\chi^2 = (R_{wP}/R_e)^2$	5.16	3.84
Ti in 4*f* (1/3, 2/3, *z*), *z*	0.5637(2)	0.5618(2)
B_{eq} (B_{iso}) 10^2 (nm^2)	0.50(1)	0.50(5)
M1 in 6*h* (*x*, 2*x*, ¼), *x*	0.1702(5)	0.1701(3)
B_{eq} (B_{iso}) 10^2 (nm^2)	0.47(5)	0.51(8)
M2 in 2*a* (0, 0, 0)		
B_{eq} (B_{iso}) 10^2 (nm^2)	0.56(6)	0.73(7)
Secondary phase	Ti_2Ni, Ti_2Ni-type *a* = 1.1127 nm	Ti_2Ni, Ti_2Ni-type *a* = 1.0954 nm
Interatomic distance (nm); standard deviations are <0.0005 nm		
Ti		
-3M1	0.2798	0.2784
-6M1	0.2802	0.2806
-3M2	0.2809	0.2808
-1Ti	0.2909	0.2936
-3Ti	0.2938	0.2927
M1		
-2M1	0.2344	0.2344
-2M2	0.2409	0.2407
-2M1	0.2452	0.2443
-2Ti	0.2798	0.2784
-4Ti	0.2802	0.2808
M2		
-6M1	0.2409	0.2407
-6Ti	0.2809	0.2806

(a) Crystal structure data are standardized using the program Structure Tidy. [51]

earlier described[26] reveal that in these compositions Ti atoms unambiguously occupy the 4*f* site, whilst (Ni,Fe)/Al atoms share the sites 2*a* and 6*h* in various mixing levels. Excess of Ti is located in the 6*h* site, consistent with the structure model of the Ti-rich Ti-Ni-Al Laves phase.[26] Similar to the Ti-Ni-Al ternary Laves phase, the isostructural four-component Ti-Fe-Ni-Al phase (λ_{FeNi}) shows a rather complicated site occupation mechanism, which reveals significant anomalies in the compositional dependences of structural parameters (Fig. 9). Lattice parameters for λ_{FeNi} show a positive deviation from linear behavior for the *a* lattice parameter but negative deviation for the *c* parameter, resulting in an almost linear change of the unit cell volume. It has to be noted that a similar behavior was observed for $Ti(Mn_{1-x}Al_x)_2$.[50] The pronounced minimum in the dependence for the *z* parameter of the Ti-Fe-Ni-Al Laves phase versus Ni-content in Fig. 9 was confirmed on two single crystals with compositions $Ti_{33.7}Fe_{10.8}Ni_{13.3}Al_{42.2}$ and $Ti_{33.6}Fe_{7.2}Ni_{20.0}Al_{39.2}$. Attempts to force positional parameters to follow a linear dependency (dotted lines in Fig. 9) did not give sufficient reason to speculate about any anomalous behavior for the *x* parameter. However, a similar approach for the *z* parameter revealed unacceptable reliability factors above 7% and residual densities of about 7 to 8 electrons/Å^3. The anomalous behavior of the atomic coordinates in the quaternary Laves phase relates to that for ternary Ti-Ni-Al[26] and probably originates from the complex substitution mechanism implying the coexistence of more than two sorts of atoms in the 6*h* site. The combined effects from atomic coordinates and unit cell dimensions are reflected on the interatomic distances $d_{Ti\text{-}3M1}$, $d_{Ti\text{-}3Ti}$, and $d_{Ti\text{-}1Ti}$. The compositional dependences of distances $d_{Ti\text{-}3M1}$ and $d_{Ti\text{-}3Ti}$ show behavior similar to the *z* parameter, while $d_{Ti\text{-}1Ti}$ follows the dependency of the *a* lattice parameter.

4.3.2 The G Phase with Th_6Mn_{23}-Derivative Type. In view of (a) the large extension of the G phase region into the quaternary system and (b) the reduced symmetry ($F\bar{4}3m$) for Ti-rich compositions in G-Ti-Fe-Al,[33] the crystal structure of the alloy $Ti_{33.33}Fe_{13.33}Ni_{10.67}Al_{42.67}$ annealed at 900 °C was studied in detail. As Rietveld refinement of XPD data was insufficient to test for the loss of centrosymmetry, neutron diffraction was employed to particularly elucidate the Ti atom site preference. Indeed, the negative neutron scattering lengths for natural titanium prompted atom ordering among Al and Ti atoms in the M6 and M6# sites in favor of the low symmetry model in space group type$F\bar{4}3m$ (Table 4). The refinement shows that (i) the M1 site is shared by Ni and Al atoms, (ii) the M2 site is occupied by Al and a small amount of Ni atoms, (iii) the M3, M4, and M5 sites accept Fe(Ni), Ti, and Al atoms, respectively, and (iv) the M5#, M6, and M6# sites are occupied by Ti and Al at various Al/Ti ratios.

5. Conclusion

Employing XPD data and EPMA the homogeneity ranges of the Laves phases and phase relations concerning the Laves phases were established in the quaternary system Ti-Fe-Ni-Al at 900 °C. A partial isothermal section $TiFe_2$-$TiAl_2$-$TiNi_2$ was constructed, and a connectivity scheme, derived for equilibria involving Laves phases in the Ti-Fe-Ni-Al quaternary system at 900 °C, was presented revealing the relative locations of Laves phases, G phase, Heusler phase, and CsCl-type phase as well as the associated tie-tetrahedra in the quaternary for 900 °C. Although at higher temperatures the Laves phase forms a continuous solid solution, two separate

Table 3 Structural data for selected compositions from the quaternary Ti-Fe-Ni-Al system ($MgZn_2$-Laves type, $P6_3/mmc$) (Data collection: D5000; radiation: Cu Kα; 2θ range: 18 ≤ 2θ ≤ 110) (a)

Parameter/ Compound	$Ti_{33.7}Fe_{13.3}Ni_{10.8}Al_{42.2}$	$Ti_{34.9}Fe_{13.3}Ni_{14.4}Al_{37.4}$	$Ti_{37.4}Fe_{13.3}Ni_{16.2}Al_{33.1}$
Heat treatment	As-cast	As-cast	As-cast
Composition from refinement	$Ti_{33.3}(Fe,Ni)_{24.2}Al_{42.5}$	$Ti_{34.9}(Fe,Ni)_{27.5}Al_{37.6}$	$Ti_{37.4}(Fe,Ni)_{28.5}Al_{34.1}$
a, nm	0.50094(5)	0.49968(3)	0.49896(4)
c, nm	0.80904(6)	0.80320(8)	0.80134(8)
V, nm^3	0.17582(3)	0.17367(2)	0.17277(3)
ρ_x, Mgm^{-3}	4.67	4.83	4.92
Reflections measured	60	62	62
Number of variables	23	25	25
$R_F = \Sigma\lvert F_o - F_c\rvert / \Sigma F_o$	0.058	0.078	0.059
$R_I = \Sigma\lvert I_o - I_c\rvert / \Sigma I_o$	0.042	0.063	0.049
$R_{wP} = [\Sigma w_i \lvert y_{oi} - y_{ci}\rvert^2 / \Sigma w_i \lvert y_{oi}\rvert^2]^{1/2}$	0.116	0.143	0.066
$R_P = \Sigma\lvert y_{oi} - y_{ci}\rvert / \Sigma\lvert y_{oi}\rvert$	0.086	0.108	0.050
$R_e = [(N - P + C)/(\Sigma w_i y^2_{oi})]^{1/2}$	0.047	0.062	0.033
$\chi^2 = (R_{wP}/R_e)^2$	6.13	5.26	3.94
Ti, 4*f* (1/3, 2/3, *z*), *z*	0.5627(2)	0.5623(2)	0.5633(2)
B_{eq} (B_{iso}) 10^2 (nm^2)	0.53(5)	0.41(5)	0.45(6)
M1 6*h* (*x*, 2*x*, ¼), *x*	0.1710(5)	0.1712(5)	0.1708(5)
Occ.	2.16(4) (Fe,Ni) + 3.84 Al	2.41(4) (Fe,Ni) + 0.19 Ti + 3.4 Al	2.51 (4)(Fe,Ni) + 0.49 Ti + 3.00 Al
B_{eq} (B_{iso}) 10^2 (nm^2)	0.44(5)	0.53(5)	0.50(6)
M2, 2*a* (0, 0, 0), Occ.	0.72(2) (Fe,Ni) + 1.28 Al	0.88(2) (Fe,Ni) + 1.12 Al	0.90(2) (Fe,Ni) + 1.10 Al
B_{eq} (B_{iso}) 10^2 (nm^2)	0.60(8)	0.66(8)	0.30(9)
Secondary phase		G phase a = 1.14231 nm	Ti_3Al
Interatomic distance (nm); standard deviations are <0.0005 nm			
Ti			
-3M1	0.2895	0.2874	0.2876
-6M1	0.2928	0.2918	0.2909
-3M2	0.2936	0.2928	0.2925
-1Ti	0.3031	0.3015	0.2992
-3Ti	0.3065	0.3053	0.3054
M1			
-2M1	0.2440	0.2430	0.2432
-2M2	0.2508	0.2495	0.2488
-2M1	0.2570	0.2566	0.2557
-2Ti	0.2895	0.2874	0.2877
4Ti	0.2928	0.2918	0.2909
M2-6M1	0.2508	0.2495	0.2488
-6Ti	0.2936	0.2928	0.2925

(a) Crystal structure data are standardized using the program Structure Tidy.[51]

homogeneity fields of $TiFe_2$-based and $Ti(TiNiAl)_2$-based Laves phases appear at 900 °C. Due to the high stability of Heusler and G phase the solid solubility of fourth elements in both the λ_{Fe} and λ_{Ni} Laves phase is limited at 900 °C and is dependent on the ternary Laves phase composition. A maximum solubility of about 8 at.% Ni is reached for the composition $Ti_{33.3}Fe_{33.3}Al_{33.4}$.

A $MgZn_2$-type structure was established for the Ti-Fe-Ni ternary and the Ti-Fe-Ni-Al quaternary Laves phase (space group: $P6_3/mmc$). Ti atoms occupy the 4*f* site, and additional Ti (for compositions higher than 33.3 at.% Ti) preferably enter the 6*h* site. Al and (Fe,Ni) share the 6*h* and the 2*a* site. For the quaternary cubic G phase, a centrosymmetric as well as a noncentrosymmetric variety was observed depending on composition: from combined x-ray and neutron powder diffraction $Ti_{33.33}Fe_{13.33}Ni_{10.67}Al_{42.67}$ was found to adopt the lower symmetry with space group $F\bar{4}3m$.

Table 4 Structural data for the G-phase in the Ti-Fe-Ni-Al system. Comparison of Rietveld refinement of x-ray and neutron powder diffraction data for the two structure models of low and high symmetry

Parameter/Alloy composition	$Ti_{33.33}Fe_{13.33}Ni_{10.67}Al_{42.67}$(a)	$Ti_{33.33}Fe_{13.33}Ni_{10.67}Al_{42.67}$(a)	$Ti_{33.33}Fe_{13.33}Ni_{10.67}Al_{42.67}$(b)
Formula from refinement (at.%)	$Ti_{32.9}Fe_{13.3}Ni_{10.6}Al_{43.2}$	$Ti_{32.8}Fe_{13.3}Ni_{10.5}Al_{43.4}$	$Ti_{33.1}Fe_{13.3}Ni_{10.4}Al_{43.2}$
Space group	$Fm\bar{3}m$	$Fm\bar{3}m$	$F\bar{4}3m$
Radiation	X-ray, Cu $K\alpha_1$	$\lambda_{neutrons}$ = 1.88570 nm	$\lambda_{neutrons}$ = 1.88570 nm
a, nm, (Guinier)	1.20124(4)	1.20124(4)	1.20124(4)
2θ range	10 ≤ 2θ ≤ 100	10 ≤ 2θ ≤ 164	10 ≤ 2θ ≤ 164
Reflections in refinement	83	79	79
Number of variables	27	20	29
$R_F = \Sigma\|F_o - F_c\|/\Sigma F_o$	0.060	0.031	0.015
$R_I = \Sigma\|I_o - I_c\|/\Sigma I_o$	0.065	0.033	0.017
$R_{wP} = [\Sigma w_i\|y_{oi} - y_{ci}\|^2/\Sigma w_i\|y_{oi}\|^2]^{1/2}$	0.098	0.059	0.049
$R_P = \Sigma\|y_{oi} - y_{ci}\|/\Sigma\|y_{oi}\|$	0.074	0.044	0.037
$R_e = [(N - P + C)/\Sigma w_i y^2_{oi})]^{1/2}$	0.049	0.027	0.027
$\chi^2 = (R_{wP}/R_e)^2$	3.96	4.77	3.36
M1; occ.	4*a* (0,0,0); 4.00 Ni	4*a* (0,0,0); 4.00 Ni	4*a* (0,0,0); 3.65(5) Ni + 0.35 Al
B_{iso} (10^2 nm^2)	0.5(1)	0.22(5)	0.26(7)
M2	4*b* (½,½,½)	4*b* (½,½,½)	4*b* (½,½,½)
occ.	3.27(6) Al + 0.73 Ni	3.45(4) Al + 0.55 Ni	3.24 Al + 0.76(4) Ni
B_{iso} (10^2 nm^2)	0.4(2)	0.6(1)	0.8(1)
M3,	24*d* (0,¼,¼)	24*d* (0,¼,¼)	24*g* (*x*,¼,¼) *x* = 0.0007(2)
occ.	16.00Fe + 8.00Ni	16.00Fe + 8.00Ni	16.00 Fe + 8.00 Ni
B_{iso} (10^2 nm^2)	0.40(5)	0.44(2)	0.35(2)
M4 (Ti)	24*e* (*x*,0,0); *x* = 0.2894(1)	24*e* (*x*,0,0); *x* = 0.2875(2)	24*f* (*x*,0,0); *x* = 0.2879(2)
occ.	24.00 Ti	24.00 Ti	24.00 Ti
B_{iso} (10^2 nm^2)	0.82(6)	0.10(8)	0.47(9)
M5 (Al)	32*f* (*x*,*x*,*x*); *x* = 0.3419 (1)	32*f* (*x*,*x*,*x*); *x* = 0.3420(2)	16*e* (*x*,*x*,*x*); *x* = 0.3416(4)
occ.	32.00Al	32.00Al	16.00 Al
B_{iso} (10^2 nm^2)	0.48(8)	0.42(6)	0.1(1)
M5#			16*e* (*x*,*x*,*x*); *x* = 0.6581(4)
occ.			15.4(1) Al + 0.6 Ti
B_{iso} (10^2 nm^2)			0.7(1)
M6	32*f* (*x*,*x*,*x*); *x* = 0.1200(1)	32*f* (*x*,*x*,*x*); x = 0.1130(28)	16*e* (*x*,*x*,*x*); *x* = 0.1197(6)
occ.	15.46(6) Ti + 16.54 Al	15.30(9) Ti + 16.70 Al	13.8(1) Ti + 2.2 Al
B_{iso}	0.44(6)	0.5(9)	0.5(3)
M6#			16*e* (*x*,*x*,*x*); 0.8792(6)
occ.			1.6(2) Ti + 14.4 Al
B_{iso}			0.5(2)
Interatomic distances (nm); standard deviations generally are < 0.0005			
M1			
-8M6:	0.2497	0.2351	**-4M6:** 0.2490
-6M4:	0.3476	0.3453	**-4M6#:** 0.2513
			-6M4: 0.3458
M2			
-6M4:	0.2530	0.2553	**-6M4:** 0.2548
-8M5:	0.3289	0.3287	**-4M5:** 0.3289
			-4M5#: 0.3298
M3			
-6M5:	0.2458	0.2459	**-2M5:** 0.2451
			-2M5#: 0.2464
-4M6:	0.2637	0.2694	**-2M6#:** 0.2626
			-2M6: 0.2644
-4M4:	0.3040	0.3037	**-4M4:** 0.3037
M4			
-1M2:	0.2530	0.2553	**-1M2:** 0.2548
-4M5:	0.2759	0.2763	**-2M5:** 02763

Table 4 Continued

Parameter/Alloy composition	$Ti_{33.33}Fe_{13.33}Ni_{10.67}Al_{42.67}$(a)	$Ti_{33.33}Fe_{13.33}Ni_{10.67}Al_{42.67}$(a)	$Ti_{33.33}Fe_{13.33}Ni_{10.67}Al_{42.67}$(b)	
-4M6:	0.2880	0.2842	**-2M5#:** 0.2767	
			-2M6: 0.2867	
-4M3:	0.3040	0.3037	**-2M6#:** 0.2890	
			-4M3: 0.3037	
M5				
-3M3:	0.2458	0.2459	0.2451	M5# -3M3: 0.2452
-3M6:	0.2743	0.2763	0.2745	-3M6#: 0.2730
-3M4:	0.2759	0.2855	0.2767	-3M4: 0.2763
-3M5:	0.3122	0.3126	0.3112	-3M5#: 0.3122
-1M2:	0.3289	0.3287	0.3289	-1M2: 0.3289
M6				
-1M1:	0.2497	0.2351	0.2490	M6# -1M1: 0.2513
-3M3:	0.2637	0.2694	0.2644	-3M3: 0.2626
-3M5:	0.2743	0.2715	0.2745	-3M5#: 0.2730
-3M4:	0.2880	0.2842	0.2867	-3M6: 0.2871
-3M6:	0.2893	0.2855	0.2890	-3M4: 0.2890

(a) Crystal structure data are standardized using the program Structure Tidy.[51] (b) No standardization of the crystal structure was performed for easy comparison with the centrosymmetric structure (space group $Fm\bar{3}m$)

Acknowledgments

This work was supported by the Austrian National Science Foundation FWF projects No. P16957, P16778 and was partially performed in the Laboratory for Neutron Scattering, ETH Zurich & Paul Scherrer Institut, Villigen PSI, Switzerland. X.Y. and P.R. are grateful to the OEAD for stipends within the bilateral WTZ Austria—China, project VII.A.16.

References

1. P. Budberg and A. Prince, Aluminium-Iron-Nickel, *Ternary Alloy Systems*, G. Petzow and G. Effenberg, Eds., VCH, Weinheim, 1992, p 66-94
2. G. Ghosh, Iron-Nickel-Titanium, *Ternary Alloy Systems*, G. Petzow and S. Ilyenko, Eds., VCH, Weinheim, 1992, p 299-316
3. P. Budberg, Aluminum-Nickel-Titanium, *Ternary Alloy Systems*, G. Petzow and G. Effenberg, Eds., VCH, Weinheim, 1992, p 10-21
4. G. Ghosh, Aluminum-Iron-Titanium, *Ternary Alloys Systems*, G. Petzow and G. Effenberg, Eds., VCH, Weinheim, 1992, p 456-469
5. V. Raghavan, Al-Fe-Ni (Aluminum-Iron-Nickel), *J. Phase Equilib.*, 1994, **15**(4), p 411-413
6. F. Lechermann, M. Fähnle, and J.M. Sanchez, First-Principles Investigation of the Ni-Fe-Al System, *Intermetallics*, 2005, **13**, p 1096-1109
7. V. Raghavan, Al-Fe-Ni (Aluminum-Iron-Nickel), *J. Phase Equilib. Diffus.*, 2005, **26**(1), p 70-71
8. V. Raghavan, Al-Fe-Ni (Aluminum-Iron-Nickel), *J. Phase Equilib. Diffus.*, 2006, **27**(5), p 489-490
9. M. Palm and J. Lacaze, Assessment of the Al-Fe-Ti System, *Intermetallics*, 2006, **14**, p 1291-1303
10. L. Eleno, K. Frisk, and A. Schneider, Assessment of the Fe-Ni-Al System, *Intermetallics*, 2006, **14**, p 1276-1290
11. G. Cacciamani, J. De Keyzer, R. Ferro, U.E. Klotz, J. Lacaze, and P. Wollants, Critical Evaluation of the Fe-Ni, Fe-Ti and Fe-Ni-Ti Alloy Systems, *Intermetallics*, 2006, **14**, p 1312-1325
12. J.C. Schuster, Critical Data Evaluation of the Aluminium-Nickel-Titanium System, *Intermetallics*, 2006, **14**, p 1304-1311
13. J.C. Schuster, Z. Pan, S. Liu, F. Weitzer, and Y. Du, On the Constitution of the Ternary System Al-Ni-Ti, *Intermetallics*, 2007, **15**, p 1257-1267
14. P. Riani, G. Cacciamani, Y. Thebaut, and J. Lacaze, Phase Equilibria and Phase Transformation in the Ti-Rich Corner of the Fe-Ni-Ti System, *Intermetallics*, 2006, **14**, p 1226-1230
15. I. Chumak, K.W. Richter, and H. Ipser, The Fe-Ni-Al Phase Diagram in the Al-rich (> 50 at. % Al) Corner, *Intermetallics*, 2007, **15**, p 1416-1424
16. M. Tokuyoshi, A Study of Semihard Magnet Alloys for Latching Reed Relays, *IEEE, Trans. Magn.*, 1971, p 664
17. E. Wieser, J. Henke, M. Muller, and C. Cruz, Connection Between Structure and Magnetic Properties of a Magnetically Semi-Permanent Fe-Ni-Al-Alloy, *Phys. Status Solidi A*, 1981, **63**(2), p 487-494
18. G.J. Barton, The Structure and Magnetic Properties of the Semi-Hard Fe-Ni-Al-Ti Magnetic Alloy, *Z. Metallkde.*, 1983, **74**(3), p 146-150
19. Z.B. Zhao, R.Z. Ma, R.Y. Feng, and Z.T. Zhao, The Precipitation in Magnetically Semi-Hard Fe-Ni-Al-Ti Alloy, *J. Mater. Sci.*, 1990, **25**(2A), p 789-795
20. C.H. Tao, X.H. Zhao, S.K. Wang, S.Q. Zhang, and M.G. Yan, Effect of Ti Addition on Microstructure of Ni-Al-Fe System Alloy, *Scr. Metall. Mater.*, 1995, **32**(3), p 475-480
21. R. Kainuma, K. Urushiyama, K. Ishikawa, C.C. Jia, I. Ohnuma, and K. Ishida, Ordering and Phase Separation in b.c.c. Aluminides of the Ni-Fe-Al-Ti System, *Mater. Sci. Eng. A*, 1997, **239-240**, p 235-244
22. J.S. Kim, D.M. Li, and C.S. Lee, Alloying Effects on Superplastic Behaviour of Ti-Fe-Al-Ni Alloys, *Mater. Sci. Technol.*, 1998, **14**(7), p 676-682
23. R. Kainuma, I. Ohnuma, and K. Ishida, Partition of Alloying Elements between $\gamma(L1_2)$, $\eta(D02_4)$, $\beta(B2)$ and $H(L2_1)$ phases in the Ni-Al-Ti base systems, *J. Chim. Phys.*, 1997, **94**, p 978-985

24. Al-Fe-Ni-Ti System, in *Phase Diagrams of Quaternary Iron Alloys*, Indian Institute of Metals, 1996, p 57-61
25. X. Yan, X.Q. Chen, A. Grytsiv, V.T. Witusiewicz, P. Rogl, R. Podloucky, V. Pomjakushin, and G. Giester, Site Preference, Thermodynamic, and Magnetic Properties of the Ternary Laves Phase $Ti(Fe_{1-x}Al_x)_2$ with the Crystal Structure of the $MgZn_2$-Type, *Int. J. Mat. Res.*, 2006, **97**(4), p 450-460
26. A. Grytsiv, X.Q. Chen, V.T. Witusiewicz, P. Rogl, R. Podloucky, V. Pomjakushin, D. Maccio, A. Saccone, G. Giester, and F. Sommer, Atom Order and Thermodynamic Properties of the Ternary Laves Phase $Ti(Ti_yNi_xAl_{1-x-y})_2$, *Z. Kristallogr.*, 2006, **221**, p 334-348
27. V. Raghavan, Al-Fe-Ti (Aluminum-Iron-Titanium), *J. Phase Equilib.*, 2002, **23**(4), p 367-374
28. M. Palm, G. Inden, and N. Thomas, The Fe-Al-Ti System, *J. Phase Equilib.*, 1995, **16**(3), p 209-222
29. M. Palm, A. Gorzel, D. Letzig, and G. Sauthoff, Structure and Mechanical Properties of Ti-Al-Fe Alloys at Ambient and High Temperature, Structural Intermetallics 1997, TMS, Warrendale, PA, 1997, p 885-893
30. B. Huneau, P. Rogl, K. Zeng, R. Schid-Fetzer, M. Bohn, and J. Bauer, The Ternary System Al-Ni-Ti Part I: Isothermal Section at 900 °C: Experimental Investigation and Thermodynamic Calculation, *Intermetallics*, 1999, **7**, p 1337-1345
31. K. Zeng, R. Schmid-Fetzer, B. Huneau, P. Rogl, and J. Bauer, The Ternary System Al-Ni-Ti Part II: Thermodynamic Assessment and Experimental Investigation of Polythermal Phase Equilib., *Intermetallics*, 1999, **7**, p 1347-1359
32. J.J. Ding, P. Rogl, and H. Schmidt, Phase Relations in the Al-rich Corner of the Ti-Ni-Al System, *J. Alloys Compd.*, 2001, **317-317**, p 379-384
33. K.P. Gupta, The Fe-Ni-Ti System, *Phase Diagrams of Ternary Nickel Alloys*, Indian Institute of Metals, Calcutta, India, 1990, **1**, p 321-343
34. B.R.K. Nanda and I. Dasgupta, Electronic Structure and Magnetism in Half-Heusler Compounds, *J. Phys.: Condens. Matter.*, 2003, **15**, p 7307-7323
35. A. Grytsiv, P. Rogl, and V. Pomjakushin, Structural Transition with Loss of Symmetry in Ti-M-Al Based G-Phases (M = Fe and Co), *Intermetallics*, 2006, **14**(7), p 784-791
36. H. Fu, D. Chen, X. Cheng, T. Gao, and X. Yang, The Influence of the X Atoms and Al 3p Occupied States in $AlTiX_2$ (X = Fe, Cu, Co, Ni), *Intermetallics, Physica B*, 2007, **388**, p 303-311
37. A. Grytsiv, J.J. Ding, P. Rogl, F. Weill, B. Chevalier, J. Etourneau, G. André, F. Bourée, H. Noël, P. Hundegger, and G. Wiesinger, Crystal Chemistry of the G-phases in the Systems Ti-{Fe, Co, Ni}-Al with a Novel Filled Variant of the Th_6Mn_{23}-type, *Intermetallics*, 2003, **11**, p 351-359
38. A. Grytsiv, P. Rogl, G. Giester, and V. Pomjakushin, Crystal Chemistry of the G-Phase Region in the Ti-Co-Al System, *Intermetallics*, 2005, **13**, p 497-509
39. X. Yan, A. Grytsiv, P. Rogl, and V. Pomjakushin. The Heusler Phase Ti25(Fe50−xNix)Al25 ($0 \le x \le 50$) Structure and Constitution, *J. Phase Equilib. Diffus.*, 2008, in press
40. P. Fischer, G. Frey, M. Koch, M. Koennecke, V. Pomjakushin, J. Schefer, R. Thut, N. Schlumpf, R. Buerge, U. Greuter, S. Bondt, and E. Berruyer, High-Resolution Powder Diffractiometer HRPT for Thermal Neutrons at SINQ, *Phys. B*, 2000, **276-278**, p 146-147
41. Nonius Kappa CCD Program Package COLLECT, DENZO, SCALEPACK, SORTAV (1998) (Delft: Nonius)
42. G.M. Sheldrick 1997 SHELX-97, Program for Crystal Structure Refinement (University of Göttingen, Germany); Windows version by McArdle (National University of Ireland, Galway)
43. T. Roisnel and J. Rodríquez-Carvajal, WinPLOTR: A Windows Tool for Powder Diffraction Pattern Analysis, *Mater. Sci. Forum*, 2001, **378-381**, p 118
44. F.J.J. van Loo, J.W.G.A. Vorljik, and G.F. Bastin, Phase Relations and Diffusion Paths in the Ti-Ni-Fe System at 900 °C, *J. Less-Common Met.*, 1981, **77**, p 121-130
45. K.P. Gupta, The Fe-Ni-Ti System Update (Iron-Nickel-Titanium), *J. Phase Equilib.*, 2001, **22**(2), p 171-175
46. S. Kiuti, An X-Ray Investigation on the Ternary Equilibrium in the Iron-Nickel-Aluminium System, *Sci. Rep. Tohoku Imp. Univ.*, 1941, **29**, p 742-794
47. M. Khaidar, C.H. Allibert, and J. Driole, Phase Equilibria of the Fe-Ni-Al System for Al-Content Above 50 at.% and Crystal Structures of Some Ternary Phases, *Z. Metallkde.*, 1982, **73**(7), p 433-438
48. L.S. Palatnik and A.I. Landau, Phase Equilibria in Multicomponent Systems, Holt, Rinehart & Winston Inc., New York, Chicago, San Francisco, Toronto, London, 1964, p 270-320, translated from Kharkov State University Press, 1961
49. ATOMS V6.0 Standard Edition Key Version 1 (c) 2002 by Shape Software
50. X. Yan, X.Q. Chen, A. Grytsiv, P. Rogl, R. Podloucky, V. Pomjakushin, H. Schmidt, G. Giester, and X. Ding, On the Ternary Laves Phase $Ti(Mn_{1-x}Al_x)_2$ with $MgZn_2$-type, *Intermetallics*, 2008, **16**, p 16-26
51. E. Parthe, L. Gelato, B. Chabot, M. Penzo, K. Cenzual, and R. Gladyshevskii, *TYPIX Standardized Data and Crystal Chemical Characterization of Inorganic Structure Types*, Springer Berlin, Heidelberg, 1994